

OPEN Quantum phase transition induced by real-space topology

C. Li¹, G. Zhang², S. Lin¹ & Z. Song¹

Received: 02 August 2016 Accepted: 23 November 2016 Published: 22 December 2016 A quantum phase transition (QPT), including both topological and symmetry breaking types, is usually induced by the change of global parameters, such as external fields or global coupling constants. In this work, we demonstrate the existence of QPT induced by the real-space topology of the system. We investigate the groundstate properties of the tight-binding model on a honeycomb lattice with the torus geometry based on exact results. It is shown that the ground state experiences a second-order QPT, exhibiting the scaling behavior, when the torus switches to a tube, which reveals the connection between quantum phase and the real-space topology of the system.

Quantum phase transitions (QPTs) are of central interest both in the fields of condensed matter physics and quantum information. The transition describes an abrupt change in the ground state of a many-body system due to its quantum fluctuations. In general, a global physical parameter, such as external fields or widely distributed coupling constants may drive QPTs, including both topological¹ and symmetry breaking types². During the transition, the real-space geometry of the system is usually unchanged. A natural question is whether a change of real-space topology can induce a QPT for some peculiar cases. It is traced back to a problem in classical physics: the effect of a magnetic field on an object depends on its real-space topology (see the illustration in Fig. 1). A magnetic field affects a conducting loop via the magnetic flux, which is independent of its shape, for instance, no matter it is a metal donut or cup. However, it has no effect on a metal bar. The switch of the topology is equivalent to the sudden removal of the applied magnetic field, which may introduce a sudden change of the quantum state at zero temperature.

In this work, we demonstrate the influence of the real-space topology to the quantum phase via concrete tight-binding models on a honeycomb and square lattices, respectively. The change of the topology is presented by the value of hopping constants, which connecting the two ends of a tube. When the boundary hopping constants vary from finite to zero, a torus switches to a tube. We investigate the groundstate property as the function of the boundary coupling. Analytical and numerical results show that the ground state exhibits the scaling behavior of second-order OPTs in the honeycomb lattice, but not in the square lattice. It reveals that a geometric topological transition may induce a QPT in certain systems, which display physics beyond the current understanding of the QPT. The possible relation between QPTs and the geometric quantity in real-space may open attractive topics for different scientific communities.

Results

Graphene torus. We consider a system of noninteracting particles in a honeycomb geometry, subjected to a magnetic flux ϕ . The tight-binding model for this system can be described by the Hamiltonian

$$H = -t \sum_{m=1}^{M} \left(\sum_{n=1}^{N-1} a_{m,n}^{\dagger} a_{m,n+1} + \sum_{n=1}^{N/4} a_{m,4n}^{\dagger} a_{m+1,4n-1} + \sum_{n=1}^{N/4} a_{m,4n-3}^{\dagger} a_{m+1,4n-2} \right) - \eta t e^{i\phi} \sum_{m=1}^{M} a_{m,N}^{\dagger} a_{m,1} + \text{H.c.},$$

$$(1)$$

where $a_{m,n}$ ($a_{m,n}^{\dagger}$) annihilates (creates) an electron in site (m, n) on an $M \times N$ lattice with integer N/4 and $M \ge 3$, and obeys the periodic boundary conditions, $a_{M+1,4n-1}=a_{1,4n-1}$ and $a_{M+1,4n-2}=a_{1,4n-2}$, with $m\in[1,M],\ n\in[1,N/4]$. Parameter t is hopping integral. Here $\phi=2\pi\Phi/\Phi_0$, where Φ is the flux threading the ring, Φ_0 is the flux quantum. In Fig. 2, the geometry of the model is illustrated schematically. In this model, factor η is important, determining the boundary condition of the system. In the view of geometry, the value of η measures the topology

¹School of Physics, Nankai University, Tianjin 300071, China. ²College of Physics and Materials Science, Tianjin Normal University, Tianjin 300387, China. Correspondence and requests for materials should be addressed to Z.S. (email: songtc@nankai.edu.cn)

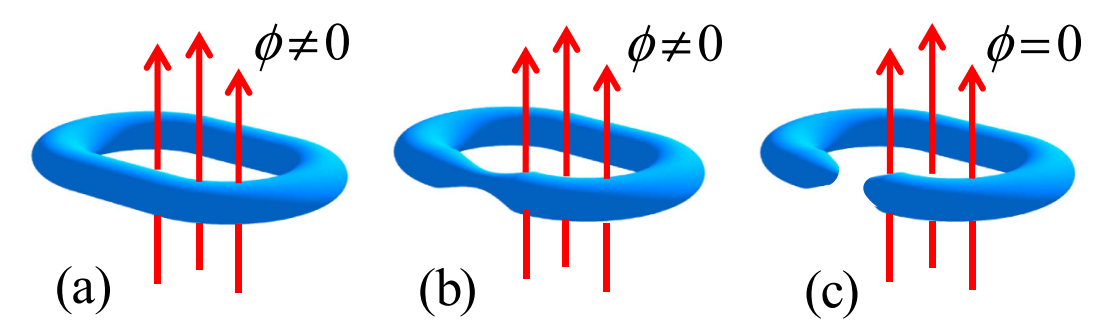


Figure 1. Schematic illustration of the aim of the present work. It arises from the fact that the effect of a magnetic field on an object depends on its real-space topology. We consider three cases: (a) A perfect torus, (b) a cut torus, (c) a broken torus. Objects in (a) and (b) have the same real-space topology, while (c) is topologically equivalent to a bar, with different real-space topology. Charged particles in systems (a) and (b) feel the same flux, while (c) cannot feel the existence of the field. The switch of the topology is equivalent to the sudden removal of the applied magnetic field, which may introduce a sudden change of the quantum state at zero temperature.

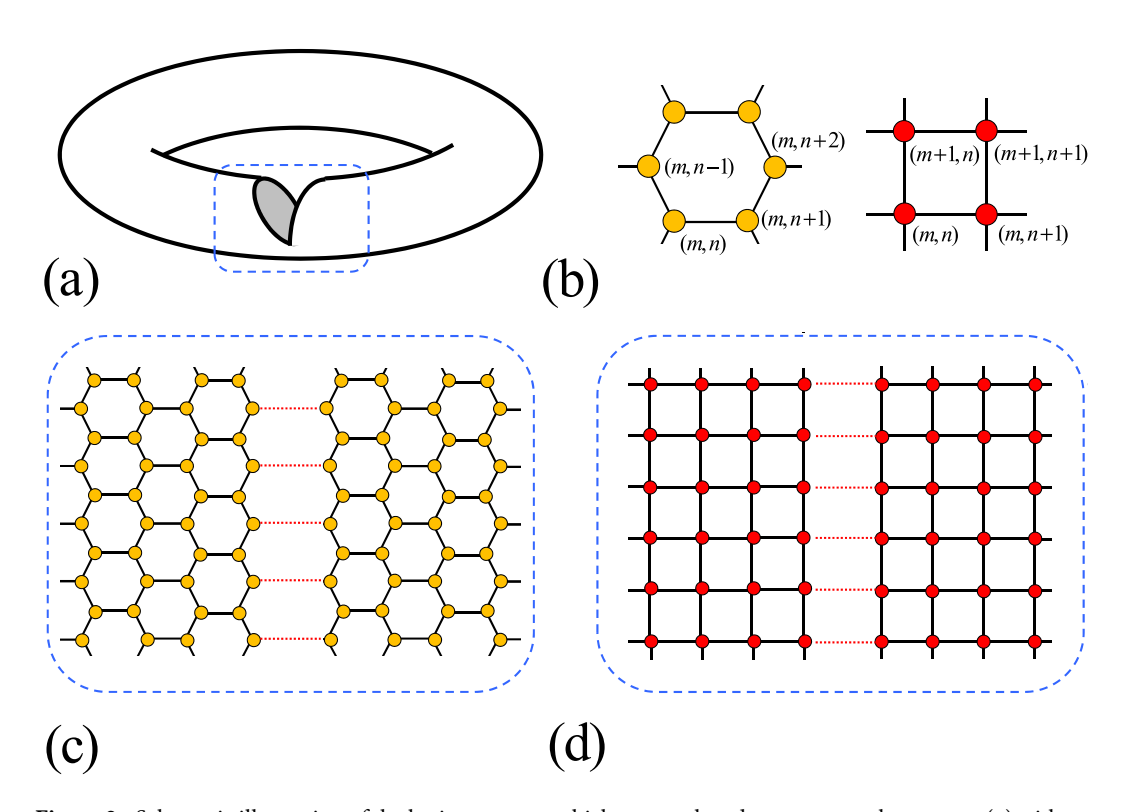


Figure 2. Schematic illustration of the lattice systems, which are employed to construct the systems (a) with different real-space topologies. We consider two types of lattices: (c) A honeycomb lattice; (d) A square lattice. A cut or broken torus is presented by the weak or zero hopping constants, which are indicated by dashed lines. The site index of two types of lattices is indicated in (b).

of the system: nonzero η corresponds to a torus whereas zero η stands for a bar. The aim of this work is to explore what happens to the ground state when η passes the zero point. To this end, exact result is preferable. We note that the value of η does not affect the translational symmetry in another direction, so we employ the Fourier transformation

$$c_{k,l}^{\dagger} = \frac{\xi_l}{\sqrt{M}} \sum_{j=1}^{M} e^{ikj} a_{j,l}^{\dagger},\tag{2}$$

to rewrite the Hamiltonian, where $\xi_l = 1$ for l = 4n, 4n - 3 and $\xi_l = e^{-ik/2}$ for l = 4n - 1, 4n - 2 with $n \in [1, N/4]$, and $k = 2\pi m/M$, $m \in [1, M]$. The Hamiltonian can be expressed as $H = \sum_k H_k$, where

$$H_{k} = -\lambda_{k} t \sum_{n=1}^{N/2} c_{k,2n-1}^{\dagger} c_{k,2n} - t \sum_{n=1}^{N/2-1} c_{k,2n}^{\dagger} c_{k,2n+1} - \eta t e^{i\phi} c_{k,N}^{\dagger} c_{k,1} + \text{H.c.}$$
(3)

Together with $[H_k, H_{k'}] = 0$, we find that H is a combination of M independent Peierls rings with the k-dependent hopping integral $\lambda_k = 2\cos(k/2)$.

The one-dimensional dimerized Peierls system at half-filling, proposed by Su, Schrieffer, and Heeger (SSH) to model polyacetylene^{3,4}, is the prototype of a topologically nontrivial band insulator with a symmetry protected topological (SPT) phase^{5,6}. In recent years, extensive studies have been received^{1,7-10}. For the open boundary condition, the number of zero modes reflects the winding number as a topological invariant, according to the bulk-boundary correspondence. Specifically, when $\eta = 0$, and infinite N, there are two zero modes if $|\lambda_k| < 1$, but not if $|\lambda_k| > 1$. Accordingly, there are approximately M/3 pairs of zero modes for a graphene tube with the open boundary condition. It indicates that the groundstate energy changes arising from the formation of the zero modes. We are interested in this process.

According to the Methods, we know that there is a pair of approximate solution for the two zero modes of Eq. (3) for small η , which are

$$\mathbf{A}_{k}^{\pm} = \frac{1}{\sqrt{2}} \left(\mp \sqrt{\frac{\eta e^{i\phi} - \lambda_{k}^{N}}{\eta e^{-i\phi} - \lambda_{k}^{N}}} \mathbf{A}_{k,0}^{+} + \mathbf{A}_{k,0}^{-} \right)$$

$$\tag{4}$$

with eigenvalues

$$\varepsilon_k^{\pm} = \pm \Omega_k^{-1} t \sqrt{(\eta - \lambda_k^N \cos \phi)^2 + \lambda_k^{2N} \sin^2 \phi}.$$
 (5)

Where

$$(\mathbf{A}_{k,0}^{\pm})^{T} = \frac{1}{\sqrt{\Omega_{k}}} \left(\alpha_{k,1}^{\pm}, \, \alpha_{k,2}^{\pm}, \, \alpha_{k,3}^{\pm}, \, ..., \alpha_{k,N}^{\pm} \right), \tag{6}$$

with $\alpha_{k,l}^+ = [1-(-1)^l]\lambda_k^{(l-1)/2}/2$, $\alpha_{k,l}^- = [1+(-1)^l]\lambda_k^{(N-l)/2}/2$ and $\Omega_k = (1-\lambda_k^{2N})/(1-\lambda_k^2) \approx (1-\lambda_k^2)^{-1}$. These analytical expressions are the base for the investigation of the quantum phase transition induced by η .

Scaling behavior. Based on the above analysis, the groundstate wavefunction can be expressed as $|\psi_{\rm g}\rangle = |\psi_{\rm b}\rangle |\psi_{\rm m}\rangle$, with energy $E_{\rm g} = E_{\rm b} + E_{\rm m}$, where $|\psi_{\rm b}\rangle$ is the lower band eigenstate with energy $E_{\rm b}$, and

$$|\psi_{\rm m}\rangle = \prod_{\{k\}} \psi_k^{\dagger} \mathbf{A}_k^{-} |0\rangle \tag{7}$$

is the midgap state with energy $E_{\rm m} = \sum_{\{k\}} \varepsilon_k^-$, where $\{k\}$ denotes the set of k within the region $2\pi/3 < k < 4\pi/3$. In the thermodynamic limit, the band state is independent of η , while the midgap state is dependent of η . To characterize the quantum phase transition induced by η , we look at the second-order derivatives of the groundstate energy

$$\frac{\partial^2 E_{\rm g}}{\partial \eta^2} \approx \frac{\partial^2 E_{\rm m}}{\partial \eta^2} = t \sin^2 \phi \sum_{\{k\}} \frac{\lambda_k^{2N}}{\Omega_k^4 (\varepsilon_k^-)^3}. \tag{8}$$

Obviously, the property of $\partial^2 E_{\mathbf{g}}/\partial \eta^2$ depends on the behavior of $\partial^2 \varepsilon_k^-/\partial \eta^2$. From the exact expression of ε_k^{\pm} in Eq. (5), we note that the gap between ε_k^+ and ε_k^- has a minimum

$$\Delta_m^k = 2t\Omega_k^{-1}\lambda_k^N|\sin\phi| \tag{9}$$

at $\eta_m^{\,k}=\,\lambda_k^{\,N}\cos\phi,$ which is obtained from $\partial\varepsilon_k^{\,\pm}/\partial\eta=\,0.$ In addition, $\partial^2\varepsilon_k^{\,-}/\partial\eta^2$ reaches the maximum

$$\left(\frac{\partial^2 \varepsilon_k^-}{\partial \eta^2}\right)_m = \frac{-t}{\lambda_k^N \Omega_k |\sin \phi|} = \frac{-2t^2}{(\Omega_k)^2 \Delta_m^k},$$
(10)

at the same point η_m^k . It is found that, quantities Δ_m^k , η_m^k , and $(\partial^2 \varepsilon_k^-/\partial \eta^2)_m$ all exhibit scaling behavior. These facts should result in the scaling behavior of $\partial^2 E_g/\partial \eta^2$. We would like to point out that, the above analysis is not applicable to the situation of $k=\pi$. In this case, we have $\lambda_k=0$, which reduces the SSH ring to a trivial case. On the other hand, in the case of $\phi\to 0$, the avoided level-crossing between ε_k^+ and ε_k^- becomes a level-crossing in a finite system. The second-order QPT becomes the first-order one.

To demonstrate the origin of the critical behavior occurs in H_k , we plot several typical band structures for H_k as functions of η in Fig. 3. It shows that in the case of $|\lambda_k| > 1$, the band structures are unchanged when the boundary condition changes no matter the flux presents or not. In the case of $|\lambda_k| < 1$, the main band structures are still unchanged when the boundary condition changes. There are two midgap levels emerge from the upper and lower

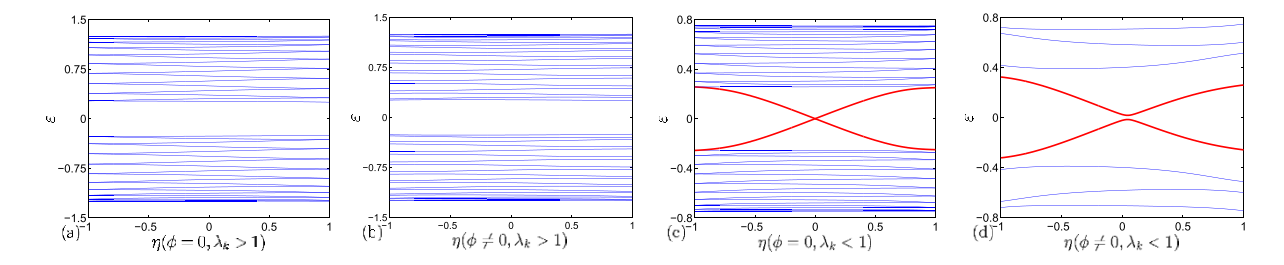


Figure 3. Energy spectra for the Hamiltonian in Eq. (3) on a lattice with N=20 for (a), (b), (c) and N=4 for (d), obtained by exact diagonalization. The parameters are (a) $\phi=0$, $\lambda_k=1.5$; (b) $\phi=\pi/4$, $\lambda_k=1.5$; (c) $\phi=0$, $\lambda_k=0.5$; (d) $\phi=\pi/4$, $\lambda_k=0.5$. We see that the zero modes do not appear in the cases of (a) and (b), no matter the flux is zero or not. In contrast, the zero modes appear as a level crossing and avoided level crossing, in the cases of (c) and (d), respectively. In the case of (d), we take a small N in order to demonstrate the avoided level-crossing clearly.

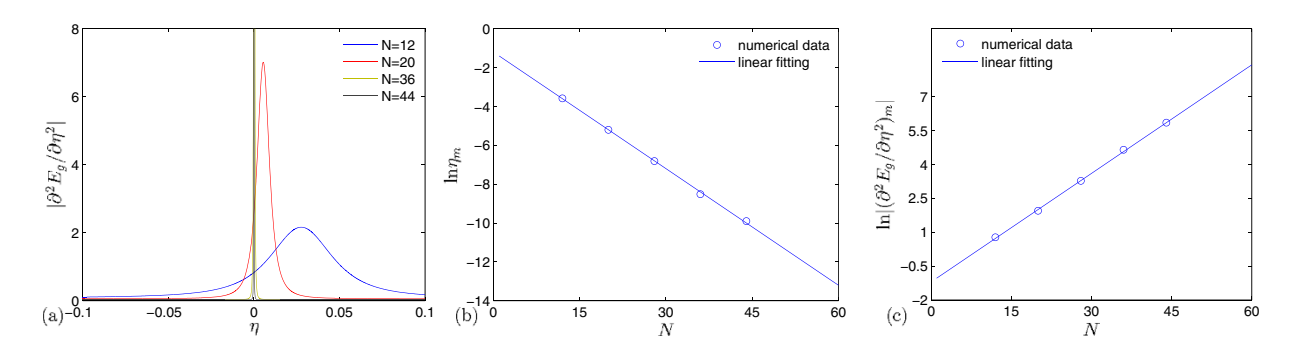


Figure 4. The characteristics of second-order QPT for the present system in Eq. (1). (a) Plots of $\partial^2 E_{\rm g}/\partial \eta^2$ as a function of η for different values of N, (b) the scaling law of pseudo critical point η_m as a function of N, (c) the scaling law of the $(\partial^2 E_{\rm g}/\partial \eta^2)_m$ as a function of N. The parameters for all plots are M=7 and $\phi=\pi/4$.

bands, respectively. The appearance of midgap levels does not depend on the flux. However, the key feature is that the flux can lead to a level-crossing. The flux takes the role of quantum fluctuation, driving the second-order QPT. We also plot the $\partial^2 E_g/\partial \eta^2$ as functions of η and N for nonzero ϕ in Fig. 4. It shows that $\partial^2 E_g/\partial \eta^2$ has a maximum $(\partial^2 E_g/\partial \eta^2)_m$ at a pseudo critical point η_m . This predicts that, in large N limit, $(\partial^2 E_g/\partial \eta^2)_m$ diverges at zero η_m . The plots of η_m and $(\partial^2 E_g/\partial \eta^2)_m$ as functions of N indicate the scaling law, exhibiting the second-order QPT behavior. The linear fitting allows us to estimate the scaling functions as the from

$$\ln \eta_m = (-0.2 \pm 0.111)N - (1.2 \pm 0.332), \tag{11}$$

$$\ln \left| \left(\frac{\partial^2 E_{\rm g}}{\partial \eta^2} \right)_m \right| = (0.16 \pm 0.077) N - (1.2 \pm 0.234), \tag{12}$$

which are in good accordance with the numerical results.

Another way of looking at QPTs from the quantum information point of view is ground-state fidelity 11,12 . For our case, we focus on the midgap-state fidelity, which is defined as

$$F(\eta, \delta) = |\langle \mathbf{A}^{+}(\eta - \delta) | \mathbf{A}^{+}(\eta + \delta) \rangle|. \tag{13}$$

A straightforward derivation results in

$$F(\eta_m, \delta) = \frac{\lambda_k^N |\sin \phi|}{\sqrt{\delta^2 + \lambda_k^{2N} \sin^2 \phi}} \approx \frac{\Omega_k \Delta_m^k}{2t |\delta|},\tag{14}$$

which also exhibits scaling law.

From above analytical and numerical analysis, we conclude that the real-space topology can induce a QPT. Key features of such kind of phase transition are that it is induced by a local parameter η , which is similar to the impurity induced QPT¹³. We would also like to point out that the flux is crucial for the transition. In the case of zero flux, the quantum transition reduces to the first-order transition. The parameter η drives the transition from one edge state to another through the quantum fluctuation of the flux. Another point we want to address is that the contexture of the toroid, honeycomb lattice, is also crucial for the QPT. We demonstrate this by the following system.

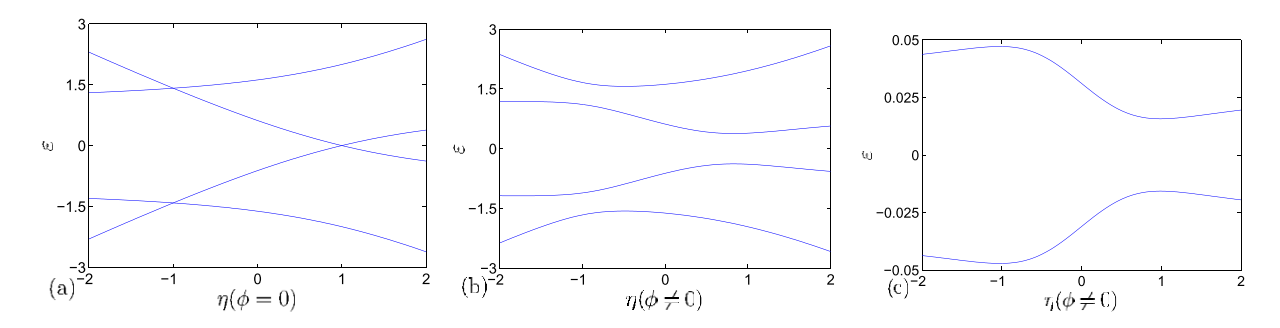


Figure 5. Energy spectra for the Hamiltonian in Eq. (23) on a lattice with N=4 for (a), (b), and N=100 for (c), which only shows the bottom energy level of the upper band and the top energy level of the lower band for simplicity, obtained by exact diagonalization. The parameters are (a) $\phi=0$; (b) $\phi=\pi/4$; (c) $\phi=\pi/4$. Here, we set $\lambda_{2k}=0$ for all figures because it is just an on-site potential and has no influence on the band structure. We see that the zero modes appear as a level crossing in the case of (a) when no flux. In contrast, in case of (b), it seems like an avoided level-crossing happens when flux presents. But in the case of (c), we demonstrate that there is still a gap between the upper and lower bands even if N is sufficiently large, which means there is no avoided level-crossing whether the flux presents or not.

In contrast to the graphene tube, we consider a system of noninteracting particles in a square lattice, subjected to a magnetic flux ϕ . The tight-binding model for this system can be described by the Hamiltonian

$$H = -t \sum_{m=1}^{M} \left(\sum_{n=1}^{N-1} a_{m,n}^{\dagger} a_{m,n+1} + \sum_{n=1}^{N} a_{m,n}^{\dagger} a_{m+1,n} \right) - \eta t e^{i\phi} \sum_{m=1}^{M} a_{m,N}^{\dagger} a_{m,1} + \text{H.c.},$$

$$(15)$$

which obeys the periodic boundary conditions, $a_{M+1,n}=a_{1,n}$. From the Methods, there is no QPT for the corresponding real-space topological change in the square lattice system. To show this point more clearly, we plot several typical band structures for H_k described in Eq. (23) as functions of η in Fig. 5. It shows that in the case of $\phi=0$, the band structures are always level-crossing, even in the small size of the system. In the case of $\phi\neq 0$, the level-crossing has been broken and a gap appears between upper and lower bands, even in the very large size of the system. This means that there is no avoided level-crossing whether flux presents or not. These two examples indicate that the occurrence of a real-space induced QPT strongly depends on the contexture of the system. It also reveals a fact that the groundstate property must be tightly connected to the topology of the system in which a real-space induced QPT can happen.

Discussion

In this work, we have demonstrated the existence of the QPT induced by the real-space topology of the system. In contrast to the conventional QPT, which is driven by a global physical parameter, such a QPT is induced by a varying local parameter. Nevertheless, the characteristics of second-order QPT, such as scaling behaviors of the second-order derivatives of groundstate energy, pseudo critical point, and the fidelity of the groundstate wavefunction, are all obtained. This finding reveals the connection between the QPT and the real-space topology, which will motivate further investigation.

Methods

The approximate solution of a Peierls ring with the k-dependent hopping integral $\lambda_k = 2\cos(k/2)$. We write down the Hamiltonian (3) in the basis $\psi_k^{\dagger} = (c_{k,1}^{\dagger}, c_{k,2}^{\dagger}, c_{k,3}^{\dagger}, ..., c_{k,N}^{\dagger})$ and see that

$$H_k = -t\psi_k^{\dagger} h_{k,N} \psi_k, \tag{16}$$

where $h_{k,N}$ represents a $N \times N$ matrix and contains two parts, $h_{k,N} = h_{k,N}^0 + h_{k,N}'$. Here two $N \times N$ matrices are

$$h_{k,N}^{0} = \begin{pmatrix} 0 & -\lambda_{k} & 0 & \cdots & 0 & 0 & \lambda_{k}^{N} \\ -\lambda_{k} & 0 & 1 & \cdots & 0 & 0 & 0 \\ 0 & 1 & 0 & \cdots & 0 & 0 & 0 \\ \vdots & \vdots & \vdots & \ddots & \vdots & \vdots & \vdots \\ 0 & 0 & 0 & \cdots & 0 & 1 & 0 \\ 0 & 0 & 0 & \cdots & 1 & 0 & -\lambda_{k} \\ \lambda_{k}^{N} & 0 & 0 & \cdots & 0 & -\lambda_{k} & 0 \end{pmatrix},$$

$$(17)$$

and

$$h'_{k,N} = \begin{pmatrix} 0 & \cdots & \eta e^{i\phi} - \lambda_k^N \\ \vdots & \ddots & \vdots \\ \eta e^{-i\phi} - \lambda_k^N & \cdots & 0 \end{pmatrix}, \tag{18}$$

respectively. It is hard to get the explicit eigenfunctions of matrix $h_{k,N}$. Fortunately, we have two eigenvectors with zero eigenvalue, i.e., $h_{k,N}^0 \mathbf{A}_{k,0}^\pm = 0$, where

$$(\mathbf{A}_{k,0}^{\pm})^{T} = \frac{1}{\sqrt{\Omega_{k}}} (\alpha_{k,1}^{\pm}, \, \alpha_{k,2}^{\pm}, \, \alpha_{k,3}^{\pm}, \, ..., \alpha_{k,N}^{\pm}), \tag{19}$$

with $\alpha_{k,l}^+ = [1-(-1)^l]\lambda_k^{(l-1)/2}/2$, $\alpha_{k,l}^- = [1+(-1)^l]\lambda_k^{(N-l)/2}/2$ and $\Omega_k = (1-\lambda_k^{2N})/(1-\lambda_k^2)\approx (1-\lambda_k^2)^{-1}$. We see that in large N limit, $h_{k,N}$ depicts an open chains: (i) $|\lambda_k| < 1$, η_k vanishes, a N-site ring becomes a N-site chain; (ii) $|\lambda_k| > 1$, η_k tends to infinity, a N-site ring reduces to a (N-2)-site chain and a 2-site separated dimer with eigenvalues out of the bands. In both two cases, there are always two zero-mode states, in which the particle probability locates around the junction, which are so-called edge states. The solutions of both cases accord with each other. The solution for $h_{k,N}$ with finite N is the basement of the scaling behavior for the geometric topological transition. Since two zero modes \mathbf{A}_0^+ are at midgap, $h_{k,N}$ can be regarded as a perturbation for small η . The degenerate perturbation method gives the

$$\mathbf{A}_{k}^{\pm} = \frac{1}{\sqrt{2}} \left(\mp \sqrt{\frac{\eta e^{i\phi} - \lambda_{k}^{N}}{\eta e^{-i\phi} - \lambda_{k}^{N}}} \mathbf{A}_{k,0}^{+} + \mathbf{A}_{k,0}^{-} \right)$$
(20)

with eigenvalues

$$\varepsilon_k^{\pm} = \pm \Omega_k^{-1} t \sqrt{(\eta - \lambda_k^N \cos \phi)^2 + \lambda_k^{2N} \sin^2 \phi}.$$
 (21)

The exact solution of the square lattice system. From the Hamiltonian (15), which obeys the periodic boundary conditions, $a_{M+1,n}=a_{1,n}$. The geometry of this system is schematically illustrated in Fig. 2(b,d). We employ the Fourier transformation

$$c_{k,l}^{\dagger} = \frac{1}{\sqrt{M}} \sum_{j=1}^{M} e^{ikj} a_{j,l}^{\dagger},$$
 (22)

to rewrite the Hamiltonian, where $k = 2\pi m/M$, $m \in [1, M]$. The Hamiltonian can be still expressed as $H = \sum_k H_k$, where

$$H_{k} = -t \sum_{n=1}^{N-1} c_{k,n}^{\dagger} c_{k,n+1} - \eta t e^{i\phi} c_{k,N}^{\dagger} c_{k,1}$$

$$+ \text{H.c.} - \lambda_{2k} t \sum_{n=1}^{N} c_{k,n}^{\dagger} c_{k,n}.$$
(23)

Together with $[H_k, H_k] = 0$ and $\lambda_{2k} = 2\cos k$, we find that H is a combination of M independent rings with the k-dependent on-site potential $-\lambda_{2k}t$. The spectra of H_k with $\eta = 1$ and 0 are

$$-2t\cos[(2\pi n + \phi)/N] - \lambda_{2k}t \tag{24}$$

and

$$-2t\cos[\pi n/(N+1)] - \lambda_{2k}t, \tag{25}$$

respectively, where $n \in [1, N]$. It indicates that the band structure is unchanged as the boundary condition changes. And several typical band structures for Eq. (23) have been plotted as functions of η in Fig. 5 to show this point clearly.

References

- Hasan, M. Z. & Kane, C. L. Colloquium: Topological insulators. Rev. Mod. Phys. 82, 3045 (2010); Qi, X.-L. & Zhang, S.-C. Topological insulators and superconductors. ibid. 83, 1057 (2011).
- 2. Sachdev, S. Quantum Phase Transitions. (Cambridge University Press, Cambridge, England, 1999).
- 3. Su, W. P., Schrieffer, J. R. & Heeger, A. J. Solitons in Polyacetylene. Phys. Rev. Lett. 42, 1698 (1979).
- 4. Schrieffer, J. R. The Lesson of Quantum Theory (North Holland, Amsterdam, 1986).
- Ryu, S. & Hatsugai, Y. Topological Origin of Zero-Energy Edge States in Particle-Hole Symmetric Systems. Phys. Rev. Lett. 89, 077002 (2002).
- 6. Wen, X.-G. Symmetry-protected topological phases in noninteracting fermion systems. Phys. Rev. B 85, 085103 (2012).
- 7. Xiao, D., Chang, M. C. & Niu, Q. Berry phase effects on electronic properties. Rev. Mod. Phys. 82, 1959 (2010).
- 8. Delplace, P., Ullmo, D. & Montambaux, G. Zak phase and the existence of edge states in graphene. Phys. Rev. B 84, 195452 (2011).
- 9. Li, L. H., Xu, Z. H. & Chen, S. Topological phases of generalized Su-Schrieffer-Heeger models. Phys. Rev. B 89, 085111 (2014).

- Li, L. H. & Chen, S. Characterization of topological phase transitions via topological properties of transition points. Phys. Rev. B 92, 085118 (2015).
- 11. Zanardi, P. & Paunkovi, N. Ground state overlap and quantum phase transitions. Phys. Rev. E 74, 031123 (2006).
- 12. Gu, S.-J. Fidelity approach to quantum phase transitions. Int. J. Mod. Phys. B 24, 4371 (2010).
- 13. Vojta, M. Impurity quantum phase transitions, *Philosophical Magazine*, **86**, 1807–1846 (2006).

Acknowledgements

We acknowledge the support of the National Basic Research Program (973 Program) of China under Grant No. 2012CB921900 and CNSF (Grant No. 11374163 and No. 11647045).

Author Contributions

C.L., G.Z. & S.L. did the derivations and edited the manuscript. Z.S. conceived the project and drafted the manuscript. All authors reviewed the manuscript.

Additional Information

Competing financial interests: The authors declare no competing financial interests.

How to cite this article: Li, C. et al. Quantum phase transition induced by real-space topology. Sci. Rep. 6, 39416; doi: 10.1038/srep39416 (2016).

Publisher's note: Springer Nature remains neutral with regard to jurisdictional claims in published maps and institutional affiliations.

This work is licensed under a Creative Commons Attribution 4.0 International License. The images or other third party material in this article are included in the article's Creative Commons license, unless indicated otherwise in the credit line; if the material is not included under the Creative Commons license, users will need to obtain permission from the license holder to reproduce the material. To view a copy of this license, visit http://creativecommons.org/licenses/by/4.0/

© The Author(s) 2016